Energy 277 (2023) 127485

Contents lists available at ScienceDirect

Energy

journal homepage: www.elsevier.com/locate/energy

An improved metaheuristic-based MPPT for centralized thermoelectric generation systems under dynamic temperature conditions

Yifeng Chen [a], Changjun Xie [a,b,c], Yang Li [a], WenChao Zhu [a,b,d,*], Lamei Xu [a,**], Hoay Beng Gooi [d]

[a] School of Automation, Wuhan University of Technology, Wuhan, 430070, China
[b] Hubei Key Laboratory of Advanced Technology for Automotive Components, Wuhan University of Technology, Wuhan, 430070, China
[c] Modern Industry College of Artificial Intelligence and New Energy Vehicles, Wuhan University of Technology, Wuhan, 430070, China
[d] School of Electrical and Electronic Engineering, Nanyang Technological University, Singapore, 639798, Singapore

ARTICLE INFO

Handling Editor: Petar Sabev Varbanov

Keywords:
Thermoelectric generator
Maximum power point tracking (MPPT)
Uneven temperature distribution
Metaheuristic algorithm
Dynamic temperature-changing conditions

ABSTRACT

This paper proposes a multi-peak maximum power point tracking (MPPT) method based on the Global Flying Squirrel Search-Particle Swarm Optimization (GFSS-PSO) for centralized thermoelectric generator (TEG) systems operating under uneven temperature distribution conditions. Conventionally, metaheuristic-based MPPT methods mainly focused on indicators such as tracking speed, oscillation amplitude, and system efficiency. However, the real-time global search ability of conventional metaheuristic-based MPPT methods designed for photovoltaic systems may not be suitable for the gradual temperature change in the thermoelectric scene. A strong global search capability also can add to the computational burden and increase the power loss in the search process. To solve these problems, the GFSS-PSO algorithm introduces improved position updating method and multi-threshold restart mechanisms to reduce energy loss and improve the dynamic performance under temperature change. The proposed method has been compared with the perturb and observe method and several state-of-the-art metaheuristic-based MPPT algorithms. Simulation results confirm that GFSS-PSO demonstrates exceptional performance and generates higher energy levels compared to perturb and observe, grey wolf optimizer, and flying squirrel search optimization methods during the search phase under dynamic temperature conditions. The improvements achieved by GFSS-PSO are remarkable, with energy levels increasing by 118.3%, 105%, and 102.2% respectively. Finally, experiments are conducted to verify the effectiveness of the proposed algorithm in a real-time digital system.

1. Introduction

1.1. Literature review

Recent years have witnessed worsening environmental pollution and increased energy costs, demanding exploring cleaner and more cost-effective energy sources [1]. As one of the feasible technologies to achieve this goal, thermoelectric generators (TEGs) are receiving growing research interest. A TEG is an energy conversion technology that directly converts thermal energy into electricity with outstanding features such as high reliability, long life, and lightweight [2].

In the medical field, wearable thermoelectric generators [3] and flexible thermoelectric generators [4] have demonstrated valuable applications. Moreover, combined heat and power systems (CHP) [5] and micro combined heat and power systems [6] have found diverse applications. Notable examples of thermoelectric hybrid systems include the proton exchange membrane (PEM) fuel cell-compound thermoelectric system [7], compressed air energy storage system [8], and ultra-low temperature PEM fuel cell power system [9].

Waste heat recovery from automobile engines has emerged as an increasingly important research topic. Hsiao YY proposes a mathematical model of a thermoelectric module for waste heat recovery [10], while Lu H conducts an experiment on the thermal uniformity and pressure drop of an exhaust heat exchanger [11]. Furthermore, the feasibility and efficiency of using exhaust gas from vehicles as a heat source for thermoelectric generators are evaluated [12].

The inherent conversion efficiency of TEG is around 7% and a single TEG has a relatively low power output, typically around 10 W [2]. Consequently, it is essential to accurately adjust the optimal electrical

* Corresponding author. School of Automation, Wuhan University of Technology, Wuhan, 430070, China.
** Corresponding author.
E-mail addresses: zhuwenchao@whut.edu.cn (W. Zhu), lmeix@163.com (L. Xu).

https://doi.org/10.1016/j.energy.2023.127485
Received 1 August 2022; Received in revised form 16 March 2023; Accepted 8 April 2023
Available online 20 April 2023

Nomenclature

α_{np}	seebeck coefficient (V/K)
U_{oc}	open-circuit voltage(V)
I_{sc}	short circuit current(A)
R_{TEG}	internal resistance(Ω)
U_{TEG}	the TEG voltage(V)
I_{TEG}	The TEG current(A)
P_{TEG}	The TEG output power(W)
R_L	load resistance(Ω)
ΔT	temperature difference(K)
I_{sci}	short-circuit current of the

ith TEG module(A)

V_{oci}	open-circuit voltage of the ith TEG module(V)
P_{TEGi}	output power of the ith TEG module(W)
R_{TEGi}	internal resistance of the ith TEG module(Ω)
GFSS	PSO parameters
δ_{avg}	average variability of the power output
δ_{max}	maximum variability of the power output
P_r	presence probability of predator
G_c	sliding constant
g_d	sliding distance

Abbreviations

TEG	thermoelectric generator
MPPT	maximum power point tracking
LMPP	local maximum power point
GMPP	global maximum power point
UTD	uneven temperature distribution
P&O	perturb and observe
PSO	Particle Swarm Optimization
GWO	grey Wolf Optimizer
FSSO	flying Squirrel Search Optimization
GFSS	global Flying Squirrel Search

operating point of the TEG to optimize the power output based on the operating conditions in different application scenarios. Maximum power point tracking (MPPT) algorithms are commonly used in TEG [13]. Due to simple construction and excellent tracking effects, perturb and observe (P&O) [14] and incremental conductance (INC) [15] are the most widely used algorithms for MPPT. By changing the operating point of the TEG, the P&O could detect the change in the output power and make control decisions. The INC considers the derivatives of the power and provides a more accurate variable of perturbation than P&O. However, the step size significantly affects the efficiency of the standard P&O and INC methods. While larger steps can achieve a faster tracking speed, they oscillate more at the steady state, resulting in higher power losses. In addition, some special methods are available for TEGs due to their linear characteristics under a constant temperature field. These methods include the open-circuit voltage (OCV) method [16] and the short-circuit current (SCC) method [17]. However, they require open-circuit or short-circuit conditions to complete the algorithm calculations, which cause additional power losses. Many works focus on improving the MPPT methods for TEGs. For example, Park J do presents an innovative way to perform the OCV measurement during the pseudonormal operation of the interfacing power electronic converter [18]. A linear extrapolation method proposed in Ref. [19] uses the linear characteristics of TEG, and it calculates the maximum power point (MPP) by relevant data from two observation points. Bond M. proposes a simple MPPT tracking circuit without current sensors [20].

A single TEG produces less electricity, and a large number of DC/DC converters will greatly increase the initial cost of the system. In practice, a centralized TEG system consists of many TEGs electrically interconnected in series or parallel and equipped with a power electronic converter. It can possess multiple MPPs in the event of uneven temperature distribution (UTD) [21]. Among them are global maximum power point (GMPP) and local maximum power point (LMPP) [22]. However, traditional MPPT methods [13–20] cannot distinguish between GMPP and LMPP, and are easily stalled on LMPP, resulting in low overall efficiency.

The centralized TEG system under UTD exhibits multi-peak characteristics similar to the photovoltaic (PV) system under partial shading conditions. The multi-peak problem in PV systems is usually solved by metaheuristics-based MPPT methods. Particle Swarm Optimization (PSO) [23], Bacteria Foraging Algorithm (BFA) [24], Grey Wolf Optimizer (GWO) [25], and Butterfly Optimization Algorithm (BOA) [26] have been successfully applied to the MPPT of PV systems under partial shading conditions. Based on the velocity vectors of the local and global best solutions, the position in the search space of the PSO in Ref. [23] is updated along the current exploration direction. However, the convergence of particles to GMPP is slowed down by the randomness in the velocity vector. The GWO randomly selects a solution with a probability function, which may help maximize exploration but also can result in long convergence times and energy losses [25]. A search space jump method [26] is proposed to improve the convergence speed of BOA by only one dynamic variable as an adjustment parameter, which reduces the complexity of the algorithm.

1.2. Research gaps and contributions

MPPT is currently being studied primarily for its tracking speed, oscillation amplitude, and system efficiency. All of which are undoubtedly crucial. Research and exploration would be more meaningful if the algorithm is improved in conjunction with the characteristics of the application scenario. As far as the centralized TEG system is concerned, it is almost impossible for the temperature field to change abruptly in the waste heat utilization scenario, which results in a continuous output power variation of the TEG system. Specifically, Cai Y studied the medium-power thermoelectric system [27], which reflects the temperature change of the hot end. Fig. 1 shows how the TEG hot end

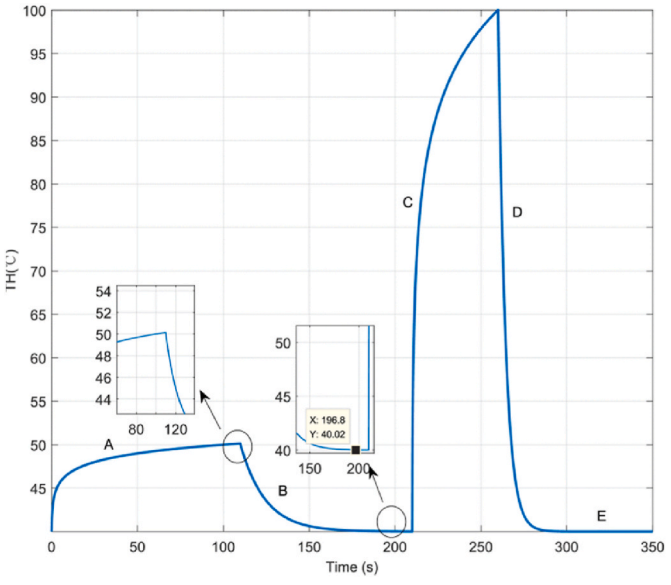

Fig. 1. Hot end temperature of the medium-power TEG system [27].

temperature (TH) varies with time during a period of 350 s. The temperature change rate is approximately 60 °C/s in Region D, where the most significant temperature drop can be observed. Several studies [21–26] only investigate the static MPPT search process under constant temperature differences or the dynamic MPPT search process focusing on the sudden step change of temperature difference. These algorithms search under the constant temperature difference after the sudden step change.

This extreme situation is unlikely to occur in the application scenario of TEG. The meta-heuristic algorithm proposed in Refs. [21–26] may have a strong global optimization ability. However, it may also become a burden if it takes a lot of time and computing resources to calculate each step. While the existing literature [21–26] has explored static and dynamic processes in the analysis of algorithm search capabilities, the current definition of dynamic processes is deemed to be overly restricted. This article aims to investigate dynamic processes in the context of TEG's practical application scenarios, offering a more comprehensive viewpoint towards optimizing algorithm searches.

Considering the temperature distributions and multi-peak characteristics of the centralized TEG system, this paper proposes a GFSS-PSO-based MPPT method with improved dynamic performance and multi-peak search capability. With the typical thermal and electrical conditions of the TEG system, several mechanisms are proposed to improve the GFFS-PSO. The main contributions of this paper are summarized as follows.

1) An improved position updating method is proposed to accurately find the GMPP in the least iterations. The configured dynamic parameters could balance the exploration time and the tracking accuracy of the tracking process.
2) To address the issue of continuous temperature change in centralized TEG systems, the proposed algorithm introduces a multi-threshold restart mechanism to overcome redundant restarts and minimize power loss.

The proposed MPPT technology is compared with advanced MPPT technologies in typical operating conditions of a centralized TEG system, and the superiority of the algorithm is demonstrated.

1.3. Paper organization

The rest of the paper is divided into four parts. Section 2 presents a model and characteristics of the TEG. Section 3 introduces the principle of MPPT technology based on GFSS-PSO. In addition, dynamic termination and multi-threshold restart mechanisms are also introduced for temperature change. A variety of typical scenarios are discussed in Section 4. Finally, real-time digital simulations are used in Section 5 to validate its hardware implementation feasibility.

2. Modeling of TEG and systems

2.1. TEG model

A TEG is a solid and semiconductor device that generates electrical power based on the Seebeck effect, as illustrated in Fig. 2(a). If there is a temperature difference between the hot and cold ends of the TEG, an electric potential can be generated and calculated by

$$V_{oc} = \alpha_{np} \times (T_h - T_c) = \alpha_{np} \times \Delta T \tag{1}$$

where α_{np} is the Seebeck coefficient of the material; T_h and T_c are the temperatures of hot and cold ends, respectively; and ΔT is the temperature difference between the hot and cold ends. The equivalent circuit of the TEG in Fig. 2(b) includes a voltage source V_{oc} and an internal resistance R_{TEG} in series. The current flowing through and the power delivered to the load R_L can be calculated as.

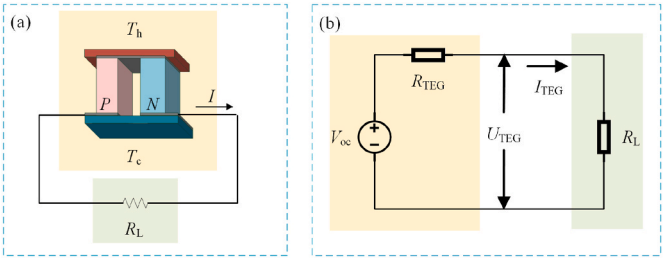

Fig. 2. Schematic diagram of (a) the Seebeck effect and (b) the equivalent circuit of the TEG.

$$I_{TEG} = \frac{V_{oc}}{(R_{TEG}+R_L)} \tag{2}$$

$$P = \frac{V_{oc}^2}{(R_{TEG}+R_L)^2} \times R_L \tag{3}$$

It can be readily obtained from (2) and (3) that the current-voltage (I–V) characteristic curve of the TEG is linear, while the power-voltage (P–V) characteristic curve is parabolic. Furthermore, the maximum power is obtained when $R_{TEG} = R_L$, and the maximum power point appears at $V_{oc}/2$ (or $I_{sc}/2$) according to the maximum power transfer theorem.

According to (1), the V_{oc} is proportional to the Seebeck coefficient α_{np}. Due to the Thomson effect, α_{np} is not a constant and would change with the temperature difference ΔT. The following equations is used to fit the nonlinear relationships of α_{np} and R_{TEG} with the temperature difference ΔT, i.e.,

$$\alpha_{np} = a\Delta T + b + c/\Delta T \tag{4}$$

$$R_{TEG} = d\Delta T^2 + e\Delta T + f \tag{5}$$

The TEG voltage U_{TEG} can thus be calculated by

$$U_{TEG} = \left(a\Delta T^2 + b\Delta T + c\right) - \left(d\Delta T^2 + e\Delta T + f\right) I_{TEG} \tag{6}$$

where a, b, c, d, e, and f are constant coefficients fitted from experimental data. I_{TEG} is output current of TEG. Table 1 shows the values of the coefficients used in this work [28].

2.2. TEG system characteristics

It is common to connect a number of TEGs to build an integrated TEG system that can accommodate wider power requirements. However, as mentioned earlier, a TEG system often operates under the UTD condition, resulting in low TEG system energy generation and efficiency [29]. Three common types of integrated TEG systems are shown in Fig. 3.

1) Centralized TEG system: the TEGs are connected in series/parallel, and the entire TEG system is controlled by a single MPPT converter. This combination has the lowest costs for converter, but it also has the most power loss under the UTD condition.
2) String-type TEG system: In this system, TEGs of the same temperature difference are connected in series to form a TEG string. Each TEG string is connected to an MPPT converter. This combination has medium-level costs for converter. The level of mismatch power loss in the case of UTD is also medium.

Table 1
The parameters of the Thermoelectric generator.

V_{OC}			R_{TEG}		
a (V/K^2)	b (V/K)	c (V)	d (Ω/K^2)	e (Ω/K)	f (Ω)
-7×10^{-5}	0.0639	−0.8536	-9×10^{-6}	0.0062	1.1972

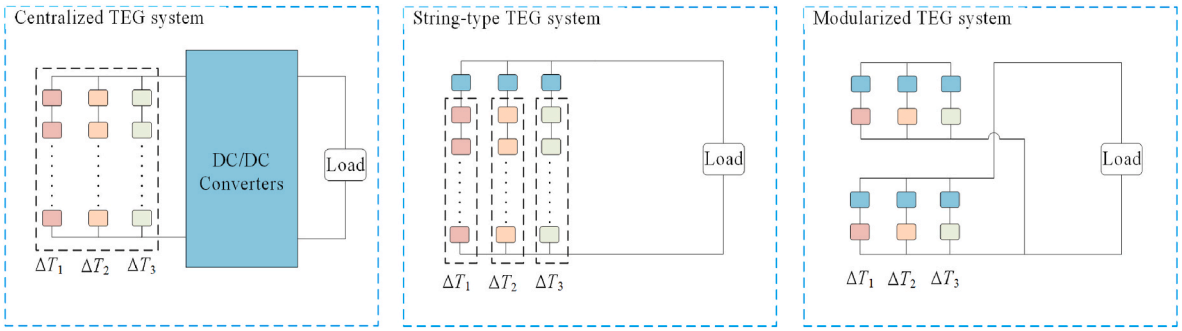

Fig. 3. Schematic diagram of three typical TEG systems.

3) Modularized TEG system: Each TEG is connected to an MPPT converter for individual MPP tracking. The power loss of the modular TEG system can be minimized at the expense of high cost for system implementation.

Despite the fact that the modularized TEG system is capable of achieving the maximum power output of each TEG, the number of MPPT converters required for this structure is too high and is rarely utilized in practice [21]. String-type TEG system is always used in recover exhaust gases from automobiles [11], with each TEG string coupled with an MPPT converter. Additionally, the temperatures of the TEGs on the same string are the same. Consequently, the MPPT algorithm is less demanding, and it is usually used in conjunction with conventional methods such as P&O and OCV. Due to the fact that only a single MPPT converter is required, the centralized structure is the most economical and worthwhile structure among the above three. The MPPT algorithm applicable to the centralized TEG system, which is the subject of this study, is most complex due to the UTD phenomenon.

A centralized TEG system is employed in this study to optimize power generation efficiency by tracking GMPP under UTD conditions. Deployment and upkeep costs of the MPPT converter can be minimized. The following is a description of the electrical model for the centralized TEG system consisting of N TEGs. The output power $P_{\mathrm{TEG}i}$ generated by the ith TEG ($i = 1, 2, \ldots, N$) and the total power P_{TEG} of all N TEGs can be calculated by

$$I_i = \begin{cases} (V_{\mathrm{oc}i} - V_{\mathrm{L}i}) \cdot \dfrac{I_{\mathrm{sc}i}}{V_{\mathrm{oc}i}} = I_{\mathrm{sc}i} - \dfrac{V_{\mathrm{L}i}}{R_{\mathrm{TEG}i}}, 0 \le V_{\mathrm{L}i} \le \dfrac{I_{oci}}{V_{oci}} \\ 0, \text{otherwise} \end{cases} \tag{7}$$

$$P_{\mathrm{TEG}i} = \begin{cases} V_{\mathrm{L}i} \cdot I_i = I_{\mathrm{sc}i} V_{\mathrm{L}i} - \dfrac{I_{\mathrm{sc}i}}{R_{\mathrm{TEG}i}} V_{\mathrm{L}i}^2, 0 \le V_{\mathrm{L}i} \le \dfrac{I_{\mathrm{sc}i}}{V_{\mathrm{oc}i}} \\ 0, \text{otherwise} \end{cases} \tag{8}$$

$$P_{\mathrm{TEG}} = \sum_{i=1}^{N} P_{\mathrm{TEG}i} \tag{9}$$

where $V_{\mathrm{oc}i}$, $I_{\mathrm{sc}i}$, $V_{\mathrm{L}i}$, and $R_{\mathrm{TEG}i}$ are the OCV, SCC, the MPPT converter output voltage, and the internal resistance of the ith TEG, respectively.

The P–V characteristic curves of the centralized TEG under different temperature distributions are shown in Fig. 4(a) and (b). The centralized TEG would present an MPP under uniform temperature distribution, as shown in Fig. 4(a). Otherwise, there would be several LMPPs and a GMPP, as shown in Fig. 4(b). To maximize the output power of the TEG, a DC-DC converter circuit should be connected between the TEG and load to ensure that the system is operating at GMPP.

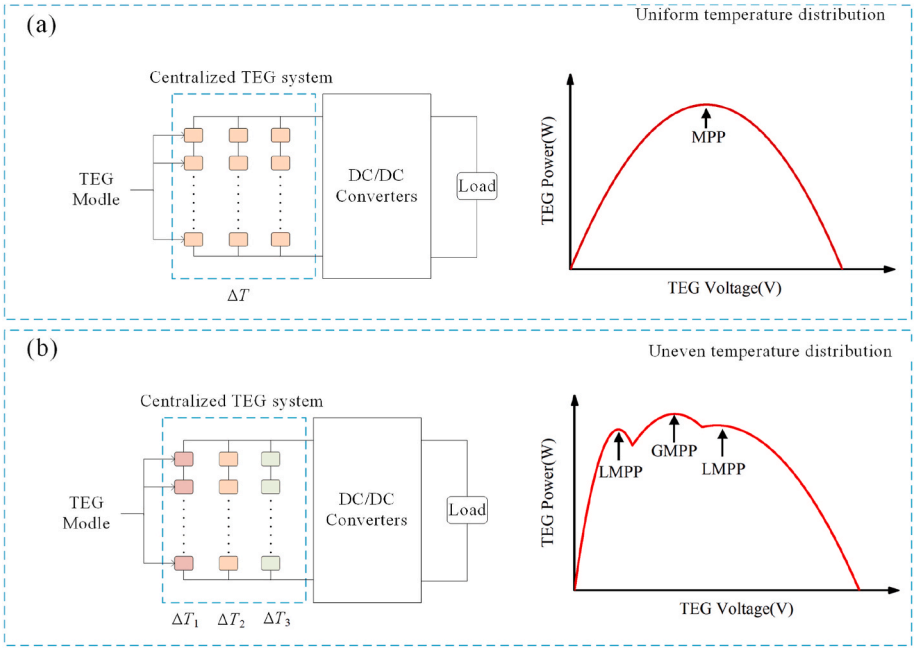

Fig. 4. Power voltage characteristic curve of TEG system under uniform temperature distribution and uneven temperature distribution.

3. Proposed MPPT algorithm

3.1. Control framework

The output characteristics of the TEG would change with the temperature difference between the two ends. At the same time, the external load may also change. The maximum power tracking process can be regarded as an impedance matching process. The impedance of the load side is adjusted by changing the duty cycle to match the dynamic internal resistance of the TEG system.

Fig. 5 illustrates the control block diagram of the MPPT system based on GFSS-PSO. This algorithm comprises three key processes, namely location update, dynamic termination, and multi-threshold restart mechanism. The real-time power serves as the input to the GFSS-PSO algorithm, while the output control signal is the real-time duty.

Control signal is connected to the input of the PWM controller, and the output of the PWM controller directly drives the switching tubes of the DC-DC converter module. When the internal resistance of the TEG changes as the temperature difference varies, the MPPT controller adjusts the duty cycle of the DC-DC converter to match the internal resistance of the TEG in real-time.

3.2. Metaheuristic-based MPPT method

Whenever the centralized TEG system faces dynamic temperature variations, some mainstream algorithms may be inapplicable. Specifically, in the standard PSO algorithm, the particles are prone to fall into the LMPP, increasing the power oscillation during the tracking process or even causing the particle to mistakenly converge to LMPP. As the external environment changes, the metaheuristic algorithm restarts the search process by detecting the power fluctuation to ensure that it can track the maximum power point in real time. However, each restart of the search causes the voltage and power to fluctuate wildly, resulting in a large energy loss. Considering the deficiencies of the Metaheuristic-based MPPT method described above, the proposed MPPT algorithm is successful in resolving these issues. The PSO and the Flying Squirrel Search Optimization (FSSO) are combined to create an improved GFSS-PSO algorithm in this section. Improved position updating mechanism, dynamic parameters, improved predator mechanism, dynamic termination conditions, and a multi-threshold restart mechanism are also proposed to improve the energy efficiency of centralized TEGs under UTD and dynamic temperature variations.

3.2.1. Particle swarm optimization

In 1995, Kennedy and Eberhart introduced the PSO algorithm [23], which is modeled after how birds find food. The bird (or particle) that finds the most food during flock foraging will share its foraging experience with other birds (or particles), and all birds (or particles) will fly to the best foraging point. PSO finds the best solution based on the continuous motion of several particles.

Fast convergence and simplicity make PSO an excellent algorithm. During the initialization of the algorithm, the position of the particles is completely random. In each new iteration, the particle determines its speed and direction based on its own experience and the experience of its group. There are two variables that influence the new positions of the particles: the best solution found by the particles themselves (P_{ibest}) and the global best solution (G_{best}). Eventually, each particle will reach the global best position by continuously adjusting its direction and velocity.

The iterative equations of the PSO are given by [23].

$$\begin{aligned} v_i^k &= \omega_i v_i^k + c_1 r_1 \left(P_{ibest}^k - d_i^k\right) + c_2 r_2 \left(G_{best} - d_i^k\right) \\ d_i^{k+1} &= d_i^k + v_i^k \end{aligned} \tag{10}$$

where d_i and v_i are the position and velocity of the ith particle. ω represents the inertia weight; c_1 and c_2 represent the self-learning factor and the social learning factor for adjusting the weight of individual and group experiences; P_{ibest} and G_{best} represent the individual and global best solutions, respectively; k represents the number of iterations; and r_1 and r_2 represent random values between 0 and 1.

PSO has a wide range of applications in MPPT. The basic steps of PSO for MPPT are as follows: Firstly, the position of N_p particles should be defined as the actual duty cycle d_i ($i = 1, 2, \ldots, N_p$). The velocity of the particle represents the next perturbation distance of the current duty cycle, and the adaptation value represents the corresponding output power. Then, the corresponding output power of each initial particle is compared, and the particle position is updated according to the iterative equations. As the particle with the highest power attracts other particles, the process will continue until all particles converge.

3.2.2. Flying squirrel search optimization

Flying Squirrel Search Optimization (FSSO) shown in Fig. 6 [28] simulates the foraging process of squirrels. Assume that the forest contains only hickory, acorn, and common trees, with one squirrel on each tree. Acorns and hickory are both considered the main food sources for squirrels. The priority levels of the three trees are as follows: the optimal solution set (hickory), the approximate solution set (acorn), and the

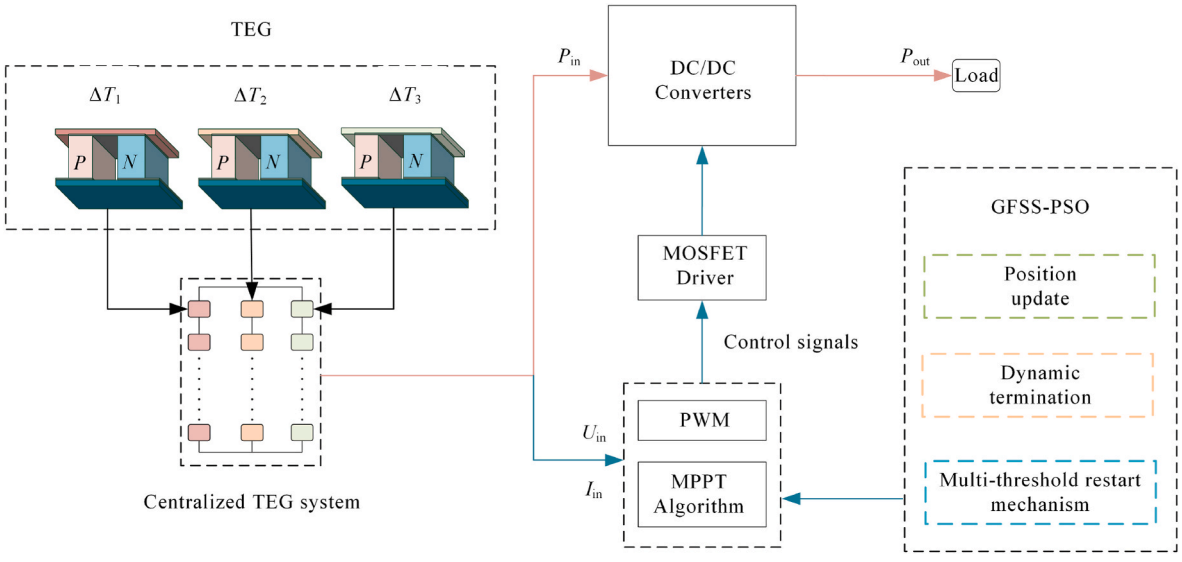

Fig. 5. Control framework of GFSS-PSO based MPPT for centralized TEG system.

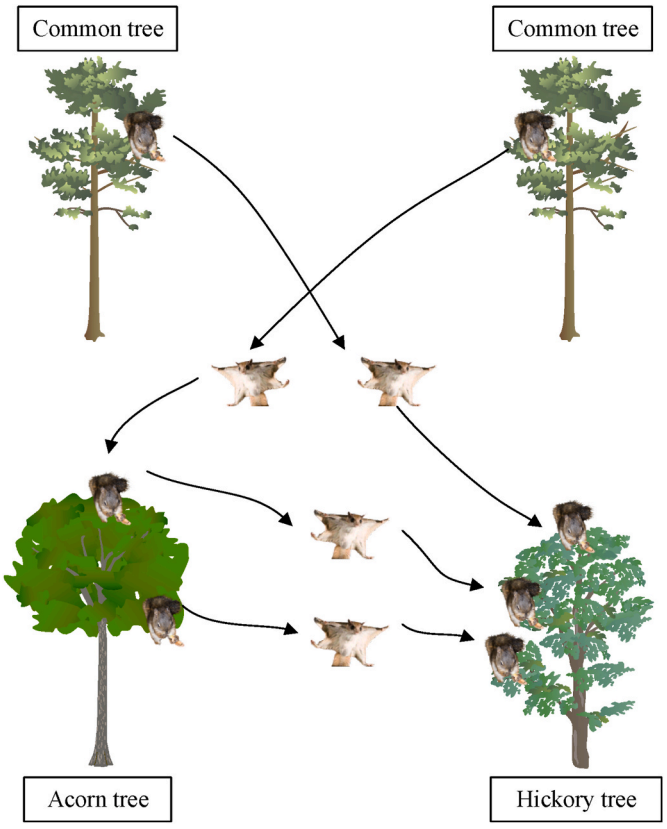

Fig. 6. Foraging behavior of flying squirrel.

common solution set (common tree).

The squirrels will randomly change positions if a predator appears. Its appearance probability is 0.1. When there is no predator present, the squirrel position is updated according to the following rules: 1) The squirrel on the hickory maintains its position; 2) Squirrel on acorn moves toward hickory; 3) Some squirrels randomly select from the common tree move toward the hickory tree, while the rest moved toward the acorn.

$$\begin{aligned} d_{at}^{k+1} &= d_{at}^{k} + g_d G_c\left(d_{ht}^{k} - d_{at}^{k}\right) \\ d_{nt}^{k+1} &= d_{nt}^{k} + g_d G_c\left(d_{ht}^{k} - d_{nt}^{k}\right) \\ d_{nt}^{k+1} &= d_{nt}^{k} + g_d G_c\left(d_{at}^{k} - d_{nt}^{k}\right) \end{aligned} \tag{11}$$

where d_{ht}, d_{at}, and d_{nt} represent squirrels on hickory, acorn, and common trees, respectively. G_c and g_d denote the sliding constant and sliding distance, respectively. In order to balance the exploitation and exploration capabilities of the algorithm, G_c is taken to be 1.9. The sliding constant g_d could be taken as a random number between [0.5,1.11] [30].

3.2.3. GFSS-PSO-based MPPT

In the basic PSO, particles may fall into the local power maximum point, which will significantly slow down the convergence time and increase power oscillations in the tracking process. And even all particles would converge to the LMPP. With reference to the position updating ways of squirrels and predators in the FSSO [24], this section introduces the GFSS-PSO-based MPPT. The maximum power tracking steps of the proposed algorithm is as follows.

1) Initialization:

Rather than randomly picking the particle positions in MPPT, the initial positions in this algorithm are fixed with uniform distribution so that the particles will not become too concentrated in the search process.

D_{min} and d_{max} are the minimum and maximum values of the duty cycle, which are taken as 0.1 and 0.9, respectively.

$$d_i^0 = 1 / \left(N_p + 1\right) \times i \quad \left(i = 1, 2, 3, \ldots N_p\right) \tag{12}$$

$$d_{min} \le d_i^k \le d_{max} \tag{13}$$

2) Position update:

a) Regular update:

By simulating the leap of a flying squirrel from a common tree to a hickory tree in the FSSO algorithm, the position updating equation of particles is as follow.

$$r = r \times \left(1 - \frac{k}{k_{max}}\right) \tag{14}$$

$$\begin{cases} d_i^{k+1} = d_i^k + \left(G_{best} - d_i^k\right) \times G_c \times g_d, \\ \quad \text{if } \left|G_{best} - d_i^k\right| - r > \text{rand}(0, r) \\ d_i^{k+1} = d_i^k + \omega_i v_i^k + c_1 r_1 \left(P_{ibest}^k - d_i^k\right) + c_2 r_2 \left(G_{best} - d_i^k\right), \\ \quad \text{if } \left|G_{best} - d_i^k\right| - r \le \text{rand}(0, r) \end{cases} \tag{15}$$

The center of the optimal environment is where the global best particle is located, and the radius of the best environment is r. The radius of the environment decreases as the number of iterations k increases. The initial radius of the optimal environment is set to 0.25. K_{max} is the parameter associated with k. The glide distance (g_d) is modified from a fixed range to a variable range. For an extensive exploration of the search space, the range of g_d is [0.5,1.11] at the beginning of the algorithm operation. To maintain convergence at subsequent stage, the range is reduced to [0.45,0.64] after the first iteration.

The first position update mode in (15) is defined as the jumping behavior. Only particles outside the range of the optimal environment have the potential to jump, and the further they are from the center of the optimal environment, the greater their probability of jumping. Within the range of the optimal environment, the particle position update equation is the PSO.

b) Improved predator mechanism:

In the FSSO, squirrels are forced to move randomly to hide when predators present. The presence probability of predator (P_r) is fixed in all iterations. As a result of this random repositioning, particles may be assigned to new and unexplored locations, increasing the capability for global exploration.

In GFSS-PSO, as the number of iterations increases, the predator presence probability P_r decreases as follows:

$$P_r = P_r \times \left(1 - \frac{k}{k_{max}}\right) \tag{16}$$

Furthermore, the random motion of the particles has been modified to (17). In this way, the random motion during the search is changed into a move toward the best position (G_{best}), which improves the convergence performance during tracking.

$$d_i^{k+1} = d_i^k + \left(G_{best} - d_i^k\right) \times \left(1 - \frac{k}{k_{max}}\right) + rand(0, r) \tag{17}$$

3) Dynamic determination:

In this paper, the following termination strategy is proposed to improve the maximum power tracking accuracy: the initial particle positions d_i are uniformly distributed in [0,1], and the particle positions become more concentrated as the PSO iterates continuously. Whenever the standard deviation of all particle positions d_i (i = 1, 2, 3, …. N_p) is

less than 0.01, the algorithm could be considered convergent and it outputs the optimal particle position G_{best}.

$$d_{avg} = (d_1 + d_2 + d_3 + . + d_n) / N_p \tag{18}$$

$$\sigma = \sqrt{\frac{1}{N}\sum_{i=1}^{N}(d_i - d_{avg})^2} < 0.01 \tag{19}$$

4)Multi-threshold restart mechanism:

In the field of thermoelectricity, TEG output characteristics and maximum power point change as the temperature difference changes. As described in Ref. [9], the GWO is restarted in response to power fluctuations caused by external changes. However, when the temperature difference continually changes, it is difficult to implement GWO in practice due to frequent restarts caused by fluctuating power and voltage.

A multi-threshold restart mechanism is used to solve these problems. External changes could be divided into the phase of severe fluctuation and phase of slow fluctuation, and GFSS-PSO is restarted using Mode A and Mode B according to the magnitude of power.

P_{TEG} represents the output power of the TEG system. P_{MPP} represents power at G_{best}. Equation (20) indicates a significant fluctuation in the TEG system's power output due to external changes. In the multi-threshold restart mechanism, the algorithm switches to Mode A. All particle positions, parameters, and variables are reassigned, and the algorithm is restarted.

$$\frac{|P_{TEG}^{'} - P_{TEG}|}{P_{TEG}} > 0.05 \tag{20}$$

As shown in (21), there is a large difference between the current power and maximum output power when the algorithm stops iterating or the power of the TEG system changes slightly. Generally speaking, the former of (21) refers to changes that have occurred in the external environment, and the latter refers to a relatively gradual change. When (21) is satisfied, the algorithm switches to Mode B. All particles are eliminated by (17), and the global and individual best positions are initialized.

$$\frac{|P_{MPP} - P_{TEG}|}{P_{MPP}} > 0.5 \quad \text{or} \quad \frac{|P_{TEG}^{'} - P_{TEG}|}{P_{TEG}} > 0.02 \tag{21}$$

3.3. Steps of the algorithm implementation

The execution steps of the GFSS-PSO algorithm are shown in Table 2, including algorithm initialization (Steps 1 and 2), iterative updates of the metaheuristic algorithm (Step 3), algorithm termination (Step 4), and algorithm restart (Step 5). In Fig. 7, the flow chart of GFSS-PSO is depicted, and the improvement mechanisms proposed in the previous section are labeled.

4. Results and discussion

A study of the MPPT performance of GFSS-PSO for a centralized TEG system under UTD is conducted by three cases, namely, start-up tests, step changes, and dynamic processes under continuous temperature changes. Frist of all, key parameters of the centralized TEG system and the connected DC-DC converter are listed in section 4.1. Then, GFSS-PSO is compared with mainstream heuristic algorithms in sections 4.2 to 4.4. Finally, a novel rating approach is presented at the end of this section to rate comprehensively the MPPT performance of these algorithms.

4.1. System and parameter configuration

The MPPT algorithm based on GFFS-PSO is simulated and evaluated by Matlab/Simulink. Various possible working conditions are simulated under three cases: Non-uniform temperature distribution, sudden changes in operating point, and continuous temperature changes. Fig. 8 shows the overall simulation model built by Matlab/Simulink 2019b and includes the centralized TEG system, boost converter, resistive load, and MPPT controller. The main parameters are as follows: Capacitance C_{in} = 100 μF, C_{out} = 100 μF; Inductance L = 300 mH, and the switching frequency is set at 20 kHz. The centralized TEG system consists of three TEG strings connected in parallel. The number of TEGs connected in series for each TEG string is n, where ΔT_1, ΔT_2, and ΔT_3 represent the temperature difference between the cold and hot sides of the respective TEG strings.

To demonstrate the effectiveness of the MPPT based on GFFS-PSO, its performance is compared with MPPT based on P&O, PSO, FSSO, and GWO. Among them, the P&O is widely used as a basic standard for performance evaluation. The PSO-based MPPT algorithm can be regarded as the evaluation and comparison standard of the metaheuristic algorithm. The GWO-based MPPT algorithm proposed by Ref. [25] only uses one tuning parameter and adds a restart mechanism for external disturbance. Thus, it can be used as a standard for dynamic tracking capabilities. FSSO is used to verify the effectiveness of the additional multi-threshold restart mechanism, improved position updating method, dynamic parameters, and improved predator mechanism.

The parameter configuration of each algorithm is the benchmark for fair performance comparison. In determining the population size, the convergence time and the oscillation time should be as balanced as possible. After several simulations, the population size of the four metaheuristic algorithms is determined to be 4 (N_p = 4). Furthermore, the tuning parameter and algorithm termination condition in the metaheuristic algorithm should be adapted to thermoelectric features. GWO and FSSO select the duty cycle uniformly distributed in the search space from 0 to 1. The maximum number of iterations is 15, and the algorithm restarts when the power difference exceeds 2%. Other parameters of each algorithm are as follows:

P&O with a fixed step size of 0.01.

Table 2
Procedure execution steps of the GFSS-PSO.

Step 1:Algorithm initialization.
The basic parameters of the GFSS-PSO algorithm are set.
Step 2: Particle initialization
Unlike the random initialization in the standard particle swarm algorithm, the proposed MPPT algorithm, its particles are initialized at fixed, equidistant points by (11).
Step 3
set k=1
FOR : i=1 to N_p
Transfer duty cycle d_i (i = 1 , 2 , 3,…N_p) to DC/DC power converter one by one.
The output voltage U and output current I of the thermoelectric module are collected in real time, and the power P_i corresponding to the current duty cycle d_i is calculated.
The positions of all particles are updated according to (13) or (15).
END FOR
Step 4
IF(Eq. (16) is satisfied)
the particle swarm iteration will be terminated, and the duty cycle D = G_{best} will be set,
and then enter step 5.
ELSE
skip to step 3.
END IF
Step 5
IF (Eq. (20) is satisfied)
Enter Mode A
The external environment changes drastically. Restart the algorithm.
ELSE IF (Eq. (21) is satisfied)
Enter Mode B
Slow transformation of the external environment occurs. Implement population elimination. All particles were eliminated using (17).
END IF

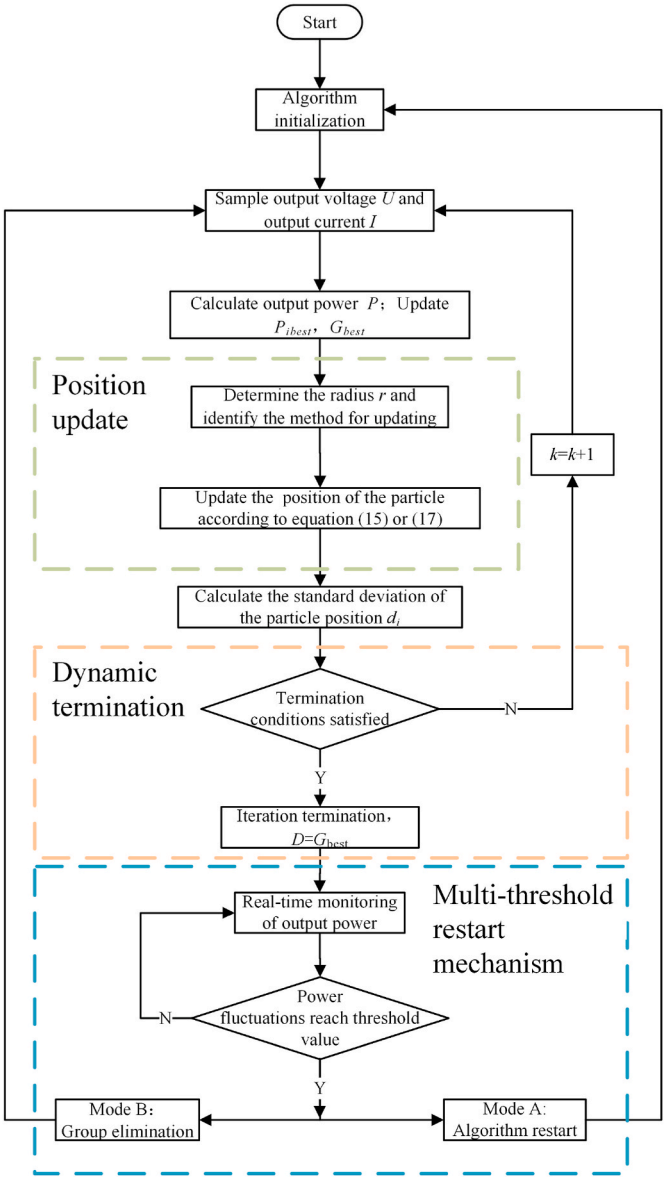

Fig. 7. Flow chart of the GFSS-PSO.

PSO[23]: w = 0.4, $C_1 = 1.2$, $C_2 = 1.6$

GWO[25]: $\alpha = 2$

FSSO[28]: $P_r = 0.1$, $G_c = 1.9$, $g_d \in [0.5, 1.11]$

There is a 0.01-s control period for all five MPPTs. Especially when the MPPT controller is controlling the boost converter, it will execute a new duty cycle every 0.01 s. MPPT technology could be mainly evaluated by several parameters such as steady-state output power, tracking time, and steady-state tracking efficiency [14]. Among them, the steady-state tracking efficiency is the ratio between steady-state output power and actual maximum output power. In addition, the power oscillation coefficient δ is introduced to evaluate the power oscillation amplitude during tracking. T represents the algorithm running time; δ_{avg} represents the average variability of the power output; and δ_{max} represents the maximum variability of the power output in (22) and (23).

$$\delta_{avg} = \frac{1}{T - 0.01} \sum_{t=0.02}^{T} \frac{|P_{TEG}(t) - P_{TEG}(t-1)|}{P_{TEG}(t-1)} \tag{22}$$

$$\delta_{max} = \max_{t \in \{0.02, 0.04, \cdots, T\}} \left\{ \frac{|P_{TEG}(t) - P_{TEG}(t-1)|}{P_{TEG}(t-1)} \right\} \tag{23}$$

4.2. Start-up under UTD condition

To simulate the case of multiple peak under UTD conditions, the temperature difference of the three TEG strings is set as $\Delta T_1 = 50$ °C, $\Delta T_2 = 100$ °C, and $\Delta T_3 = 220$ °C [22], $n = 10$. The GMPP of the centralized TEG system could reach 36.2 W, and simulation results of the five algorithms are shown in Fig. 9.

According to the final power of P&O, PSO, GWO, FSSO, and GFSS-PSO, they are 33.86 W, 32.86 W, 36.19 W, 36.19 W, and 36.19 W, respectively. GFSS-PSO is the fastest in the tracking process, taking only 0.19 s, and GWO has a tracking time of 0.49 s. Compared with GWO, the convergence time of GFSS-PSO is shortened by 61%. Tracking time by the PSO is 0.23 s, but the algorithm misconverges because the duty cycle is too concentrated after random initialization, and the tracked 32.86 W is the LMPP but not the GMPP.

Compared to the P&O algorithm, metaheuristic algorithms (GWO, FSSO, and GFSS-PSO) all collect more energy from the TEG system, indicating that they have better global search capabilities and are more suited under UTD conditions. Due to the predator mechanism of the FSSO, the particles of FSSO would gain random positions after being knocked out, significantly increasing its power oscillations. In contrast, the GFSS-PSO has the shortest tracking time and highest output energy among all algorithms. Furthermore, it is shown that the improved position updating method can enhance the global search capability of PSO. In summary, the GFSS-PSO outperforms the traditional P&O method and metaheuristic algorithms under UTD conditions.

4.3. Working point mutation

The overall working point of the centralized TEG system may change suddenly if faults of TEG occur during the operation of the thermoelectric power generation system. For the first 1 s ($\Delta T_1 = 50$ °C, $\Delta T_2 = 100$ °C, $\Delta T_3 = 220$ °C , $n = 26$), the centralized system operates steadily. A short-circuit fault of the TEGs in each TEG string simulates the working point mutation shown in Fig. 10. Similar to the previous case, the energy produced by P&O is still much smaller than that produced by other metaheuristic algorithms, suggesting that P&O could easily fall into LMPP. Without the restart mechanism, the PSO algorithm cannot adapt to changes in ambient temperature. Hence, the duty cycle output remains constant after convergence. The metaheuristic algorithms (GWO, FSSO, and GFSS-PSO) are prone to large power fluctuations because they need to restart the algorithm whenever the working point changes and approach GMPP through the exploration and development of the optimal duty cycle value. GFSS-PSO can quickly converge to a high-quality GMPP with small power fluctuations by changing the random motion in the FSSO to directional guidance within the safety circle. Further, GFSS-PSO produces more energy and has a smaller power fluctuation than FSSO, GWO, and PSO. The MPPT algorithm based on GFSS-PSO shows much higher convergence stability than other traditional intelligent algorithms, while PSO, GWO, and FSSO may not be adaptive enough to search out high-quality GMPP in a limited time.

4.4. Study on the dynamic process under continuous temperature change

In the working scenario of the TEG, the temperature of the hot end changes continually and slowly. To verify the effectiveness of the designed GFSS-PSO in dynamic conditions, this section compares simulation results for continuous temperature rise and drop under the three reference objects (P&O, GWO, and FSSO). The PSO algorithm is not compared due to the absence of dynamic restart capability.

In the simulation experiment, the temperature change rate in the first 10 s of the temperature rise and drop processes of the C section and D

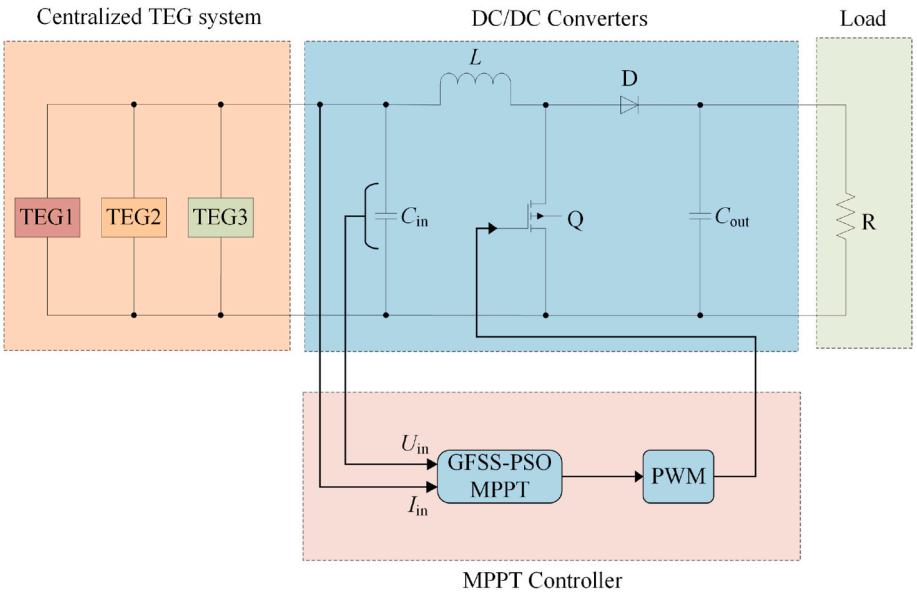

Fig. 8. Thermoelectric power generation system.

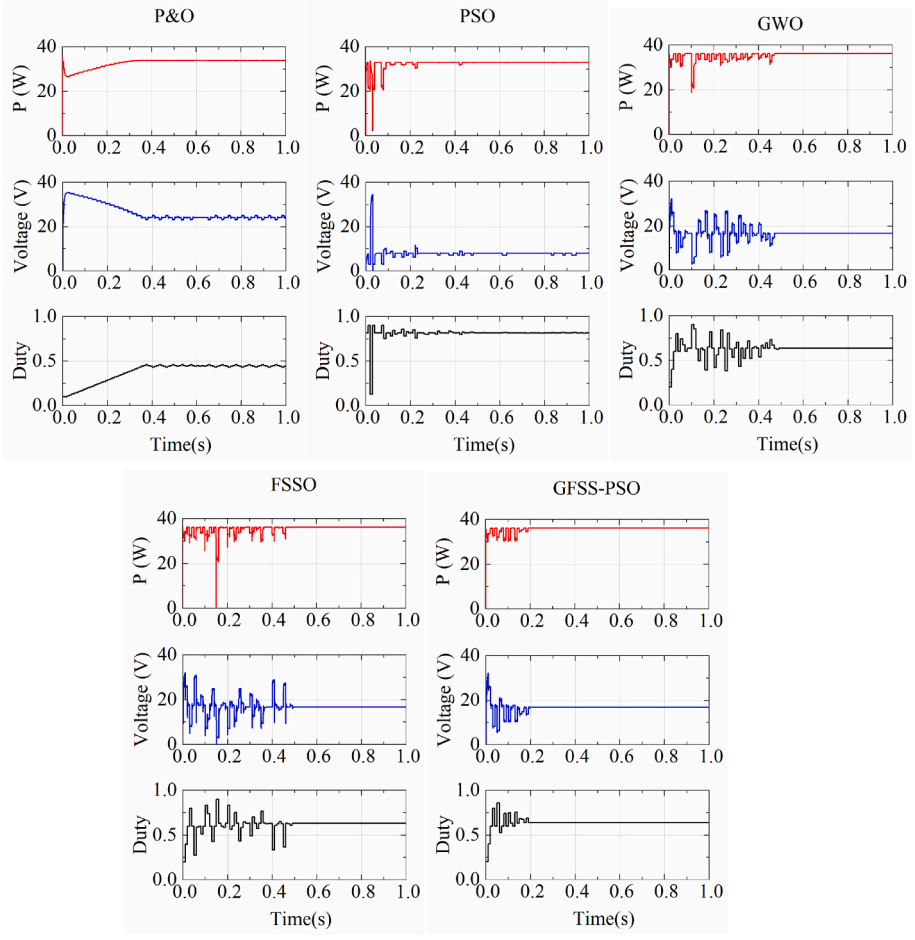

Fig. 9. MPPT tracking results of five algorithms in the case of UTD.

section (in Fig. 1) is selected to match. To better observe the power variation trend, the simulated temperature difference range is increased to [0, 300] degrees, and n is increased to 30.

1) Temperature rise process

Despite the hot end temperature of TEG slowly increasing, the position of the MPP does not change significantly. It would be very energy-

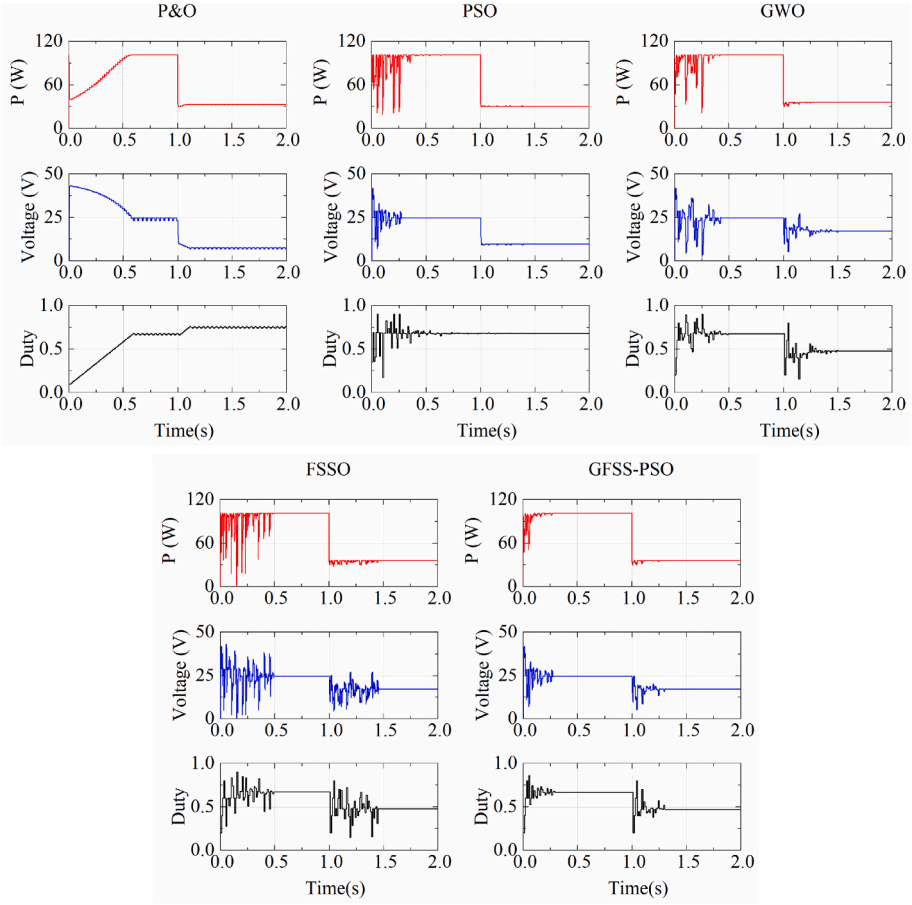

Fig. 10. MPPT tracking results of five algorithms in the case of working point mutation.

consuming to restart the algorithm frequently. As shown in Fig. 11, due to frequent restarts of the algorithm during maximum power tracking, the power of GWO fluctuates greatly. The GFSS-PSO ends the algorithm restart process in 0.747 s and enters secondary tracking in 2.79 s by multi-threshold restart mechanism (Mode B group elimination). The GWO algorithm and the GFSS-PSO complete the convergence in 5.9 s and 3.0 s, respectively, and the convergence time of GFSS-PSO is shortened by 49%.

All algorithms stop searching after 5.9 s, and the energy generated by GWO, FSSO, and GFSS-PSO at 5.9 s is 2736.73 J, 2823.26 J, and 2853.92 J, respectively. Because of the continuously increasing power of the TEG, the duty cycle of P&O is kept at 0.1, resulting in a large power loss and the lowest energy generation in the P&O. The energy generated by GFSS-PSO in the first 3 s is 118.3%, 105% and 102.2% of that generated by P&O, GWO, and FSSO, respectively, indicating GFSS-PSO can achieve convergence with less power oscillation.

As with temperature rises, the GFSS-PSO algorithm has the fastest search speed and the smallest power fluctuation of the four meta-heuristic algorithms in the temperature drop process. Temperature decreases have prevented particles from updating their historical optimal

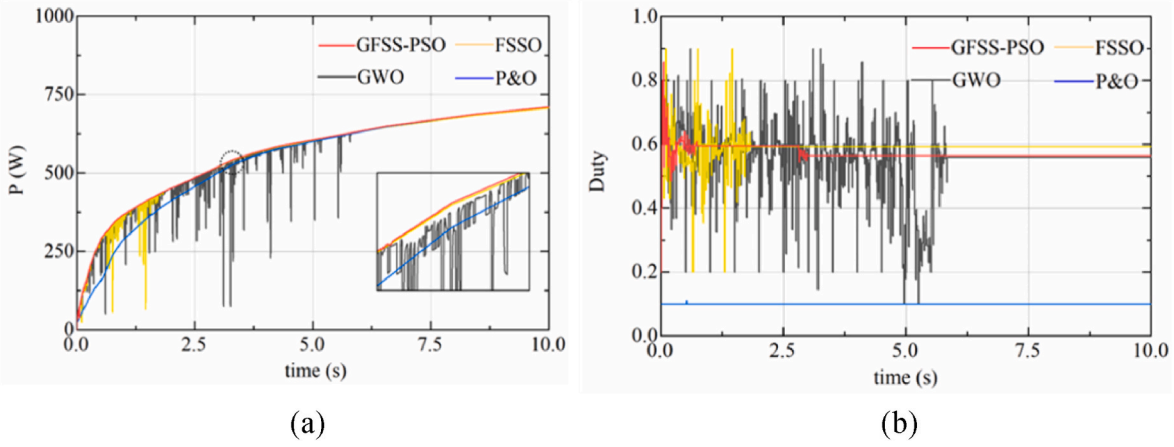

Fig. 11. Power(a) and duty(b) of P&O, PSO, GWO, and GFSS-PSO under temperature rise process.

2) The temperature drop process

positions, resulting in excessive initial position weights. In Fig. 12(b), it is evident that duty cycle values of GWO, FSSO, and GFSS-PSO come close to the error position (0.4) in the early stage of the algorithm operation (first 1 s). FSSO and GWO end the restart process of the algorithm and track to the high-quality MPP at 3.63 s and 4.26 s, respectively. Compared to GWO, the GFSS-PSO smooth transitions to the MPP through a multi-threshold restart mechanism (Mode B group elimination) in 3.40 s, cutting the convergence time by 20.2%. In the search phase (within 4.26 s), GWO, FSSO, and GFSS-PSO produced energy of 2581.62 J, 2604.69 J, and 2767.48 J, respectively. There is less power oscillation during the search phase when using GFSS-PSO to track the MPP.

As shown in Fig. 12(b), GFSS-PSO and P&O are able to respond under small continuous changes in temperature better than GWO after 5 s. Traditional P&O needs to continuously search for the best working point through constant disturbance. A multi-threshold restart mechanism is used by the GFSS-PSO algorithm to enter Mode B at 6.42 s, updating the optimal operating point within the safety circle while minimizing power fluctuations. Simulation results demonstrate that GFSS-PSO uses a multi-threshold restart mechanism to directional eliminate the population, finding the MPP with fewer fluctuations in power and faster processing times.

4.5. Analysis of MPPT results

A detailed analysis of the algorithm and its improvement mechanism is given in conjunction with the curve change trend discussed in the previous sections. To fully display characteristics of the algorithm, more detailed data are presented in Table 3 for the five algorithms in the four above cases. Six main evaluation metrics are included: steady-state tracking time, steady-state output power, generated energy, steady-state tracking efficiency, and the amplitude of maximum and average oscillation. Among them, Case 3 and Case 4 examine power tracking in the process of temperature change, so there is no relevant results at the steady state and are represented by a dash.

The MPPT results of Case 1 and Case 2 show that GFSS-PSO has the best multi-peak tracking capability, and the tracking efficiency and tracking speed are superior to those of P&O, GWO, and FSSO.

As compared with other metaheuristic algorithms, the GFSS-PSO algorithm presents the highest dynamic search capability in both rising and falling temperatures, and it finds the maximum power point with smaller power fluctuations and faster time by using a multi-threshold restart mechanism that eliminates all particles when the external temperature is constantly changing.

It is worth noting that P&O exhibited better performance than GFSS-PSO in terms of low power oscillations. To better evaluate each algorithm, a comprehensive rating analysis is introduced below.

In order to evaluate the comprehensive performance, this section determines the MPPT rating by the rated average in (24). The total achieved rating includes k_{max} termination requirements, dynamic tracking capability under temperature changes, and global search capability under UTD. And the global search capability can be subdivided into three aspects: steady-state MPPT efficiency, average steady-state tracking time, and average steady-state oscillation coefficient under start-up and mutation tests.

$$\text{MPPT RATING} = \frac{\text{Total achieved rating}}{5} \tag{24}$$

In Table 3, the performance of each indicator can be expressed by a score rating: “1” stands for the best, and 4 stands for the worst. There is a rating of “1” for average power shocks less than 5%, “2” for average shocks less than 10%, “3” for average shocks less than 20%, and “4” for average shocks greater than 20%. And this part would give a rating of “1” when the average steady-state tracking time is less than 0.2s, a rating of “2” between 0.2 and 0.4s, a rating of “3” between 0.4 and 0.6s, and a rating of “4” when it exceeds 0.6s. For the steady-state output efficiency over 99%, the score is set as “1”, “2” between 98% and 99%, “3” between 97% and 98%, and “4” below 97%. Those methods that require a termination condition k_{max} are scored “2”, otherwise “1”.

Whenever the temperature changes continuously, the P&O and PSO algorithms lose their dynamic tracking ability, and their dynamic tracking ability is rated as 4. Dynamic tracking capability ratings are based on simulation results of Case 3 and Case 4. A rating of 1 will be given if the average oscillation time and power oscillation are less than 2.5 s and 10%, respectively. Rating 2 will be given to oscillations with average oscillation times less than 5 s and average power oscillations less than 20%. Rating “3” is given when oscillation times are less than 7.5 s, and power oscillations are less than 40%.

According to the MPPT rating in Table 4, the proposed algorithm received the best rating of 1.6, followed by GWO, P&O, and FSSO with ratings of 2.4, 2.4, and 2.6, respectively, and PSO with a worse rating of 3. Due to the improved position updating method of GFSS-PSO, the search space is reduced, and a good average tracking time rating is obtained. The P&O algorithm lacks global search ability and gets the worse rating on average steady-state tracking efficiency. The GFSS-PSO also employs a multi-threshold restart algorithm for the continuous temperature changes of TEG. It greatly enhances its dynamic performance; obtains a more accurate maximum power point with less power fluctuation; and achieves the best rating for dynamic tracking.

Due to their search mechanisms, all intelligent algorithms generate large power oscillation, and P&O gets the best rating on average steady-state oscillation. Additionally, the GFFO-PSO receives the best rating in the intelligent algorithm due to the improved position updating method, which reduces power oscillation during the tracking process. At the

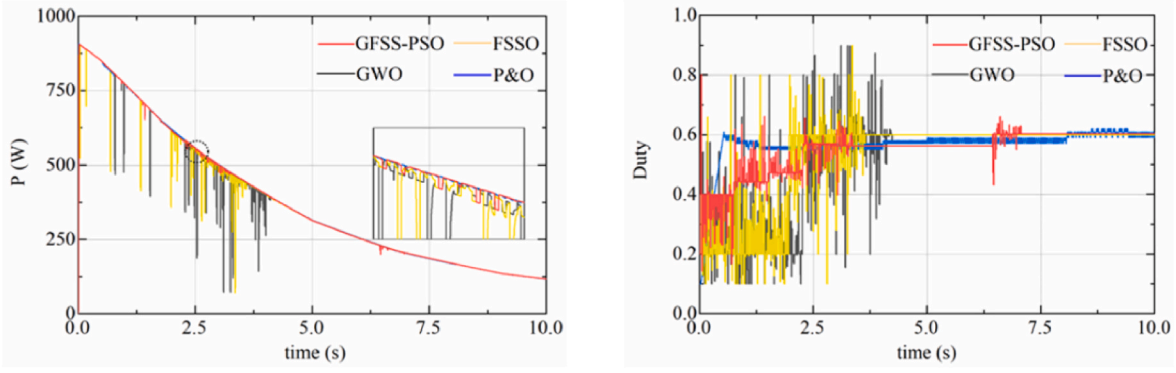

Fig. 12. (a) Power and (b) duty cycle of P&O, PSO, GWO, and GFSS-PSO algorithms under temperature drop process.

Table 3
Simulation results for various algorithms.

Algorithm	Case	Steady-state metrics			Amplitude of oscillation		Energy (J)
		Tracking time(s)	Power (W)	Efficiency	Max.	Average	
P&O	1	0.353	33.858	93.53%	2.33%	1.51%	32.78
	2	0.110	32.880	90.83%	4.6%	3.65%	115.49
	3	–	–	–	1.01%	0.21%	5417.94
	4	–	–	–	1.78%	1.23%	3881.40
PSO	1	0.231	32.864	90.78%	59.30%	11.90%	32.37
	2	–	30.112	83.18%	262.51%	29.79%	126.32
	3	–	–	–	–	–	–
	4	–	–	–	–	–	–
GWO	1	0.490	36.185	99.96%	53.07%	10.95%	35.62
	2	0.503	36.186	99.96%	94.87%	13.49%	133.3
	3	–	–	–	417.06%	45.67%	5505.55
	4	–	–	–	484.63%	32.55%	3815.77
FSSO	1	0.492	36.189	99.97%	309.78%	15.63%	35.462
	2	0.459	36.192	99.98%	455.11%	26.33%	131.76
	3	–	–	–	220.06%	35.17%	5580.99
	4	–	–	–	324.23%	25.75%	3838.83
GFSS-PSO	1	0.190	36.185	99.96%	17.98%	9.34%	35.84
	2	0.302	36.192	99.98%	49.13%	7.31%	135.6
	3	–	–	–	12.99%	2.13%	5623.59
	4	–	–	–	7.71%	2.66%	3869.59

Table 4
Simulation rating for P&O, PSO, GWO, and GFSS-PSO algorithms.

Metrics	P&O	PSO	GWO	FSSO	GFSS-PSO
Steady-state Efficiency	4	4	1	1	1
Steady-state Tracking time	2	2	3	3	2
Average steady-state oscillation	1	4	3	4	2
Dynamic tracking capability	4	4	3	3	1
k_{max}	1	1	2	2	1
MPPT rating	2.4	3	2.4	2.6	1.4

same time, GFSS-PSO can determine whether convergence is achieved by the standard deviation of particle positions, so the k_{max} termination requirement is not required.

5. Real-time digital simulation experiments

The verification of the GFFS-PSO is carried out based on RSCAD and a real-time digital simulator (RTDS). Since there is no thermoelectric model in the RSCAD library, the PV model is used to perform an alternative experiment to complete the verification of the algorithm [31]. Parameters of the PV modules, including OCV and SCC, maximum power point voltage, and maximum power point current, are set to simulate the properties of modules for thermoelectric generators. And then, the number of PV modules in series and parallel are set to simulate the structure of a centralized thermoelectric generator system. Combined with the boost circuit drive signal generator, the MPPT module has been transformed from the Simulink model and placed in the black control box in Fig. 13.

One cabinet (RACK 1) is configured in the RTDS device for real-time

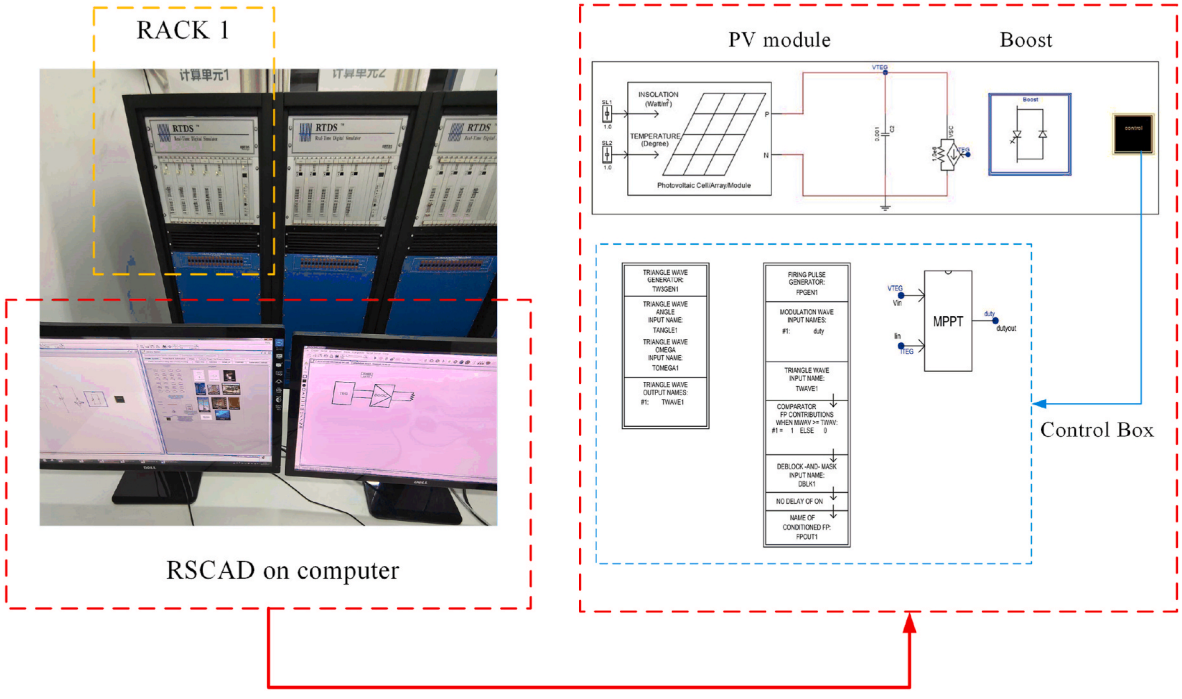

Fig. 13. Schematic diagram of RTDS experimental device.

hardware simulation calculations to perform numerical experiments of MPPT tracking under start-up test and continuous temperature rise test. These two cases can fully verify the MPPT performance under the GFSS-PSO algorithm.

Fig. 14 Shows the real-time digital simulation results for the start-up test and continuous temperature rise test. The results obtained from the simulated model are very similar to those obtained from the real-time experimental model using the RTDS setup.

In order to explain the performance difference between simulation and RTDS test results, three main reasons have been identified.

1) Delay in transmission. The RTDS test is inevitably destructive to MPPT performance when it tests input/output signal transmission.
2) Measurement interference. Since the measurement equipment does not accurately acquire the signal, continuous fluctuations occur in RTDS tests.
3) Discretization and sample holding for RTDS tests. In comparison to the simulation test, the RTDS may generate some errors.

6. Conclusion

In this paper, a dynamic multi-peak MPPT method based on the metaheuristic algorithm GFSS-PSO is proposed. In addition to solving the maximum power point tracking problem for centralized thermoelectric systems, the algorithm also accounts for continuous temperature variations and UTD conditions.

The proposed algorithm incorporates multi-peak seeking and dynamic tracking capabilities, allowing it to avoid frequent restarts and maintain effective tracking even in the presence of minor power fluctuations during continuous temperature variations. This paper presents a comparison of the P&O, GWO, and FSSO algorithms with the proposed algorithm, and analyzes the limitations of conventional algorithms when applied under continuous temperature variations. The power tracking efficiency is up to 99.9%, with average oscillations being reduced to 2% in temperature drop process. Compared to the classic P&O algorithm, the proposed method achieves an increase of 10% in power generation. Additionally, it achieves a significantly faster tracking time compared to the GWO algorithm, with a 20–40% improvement. The main contributions are as follows.

1) Compared to the classical P&O method, the GFSS-PSO algorithm is capable of consistently tracking the GMPP for the centralized TEG system under UTD.
2) The GFSS-PSO algorithm, with its improved position updating method and predator mechanism, outperforms typical metaheuristic algorithms such as PSO, GWO, and FSSO in terms of dynamic performance for MPPT. Its advanced configuration allows for faster convergence and more efficient power generation.
3) In view of the continuous temperature-changing characteristics of the TEG system, GFSS-PSO adds a multi-threshold restart mechanism to reduce the power loss caused by frequent searches of the metaheuristic-based MPPT methods.

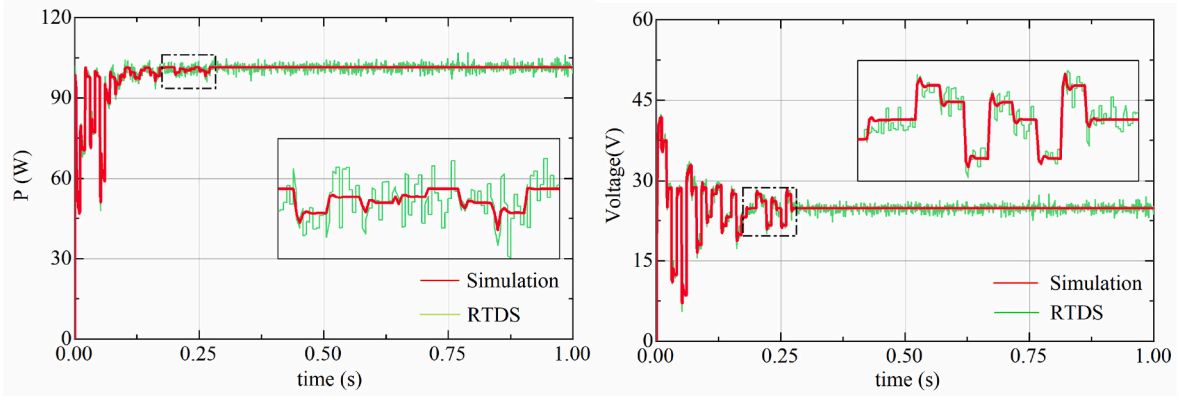

(a) The start-up test

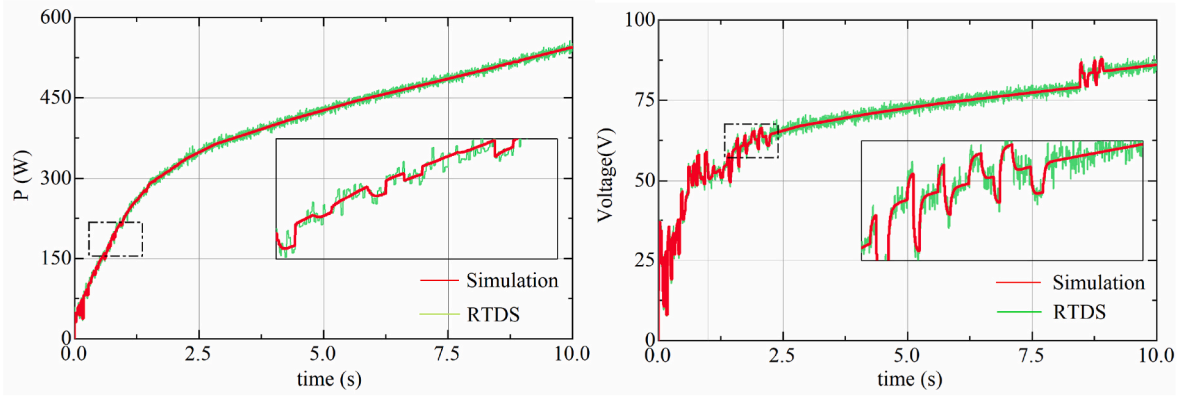

(b) Continuous temperature rise test

Fig. 14. Real-time digital simulation results for the two cases.

4) To achieve a comprehensive rating of each algorithm under various indicators, a comprehensive rating method is proposed, and the GFSS-PSO gets the best rating.

Author contributions

Conceptualization, Lamei Xu and Wenchao Zhu; Data curation, Yifeng Chen and Wenchao Zhu; Formal analysis, Hoay Beng Gooi and Yang Li; Funding acquisition, Changjun Xie; Investigation, Wenchao Zhu and Yifeng Chen; Methodology, Wenchao Zhu and Yang Li; Project administration, Ying Shi and.

Hoay Beng Gooi; Software, Lamei Xu; Supervision, Changjun Xie and Hoay Beng Gooi; Validation, Lamei Xu and Yifeng Chen; Writing – original draft, Yifeng Chen and Wenchao Zhu; Writing – review & editing, Hoay Beng Gooi and Yang Li

Declaration of competing interest

The authors declare that they have no known competing financial interests or personal relationships that could have appeared to influence the work reported in this paper.

Data availability

Data will be made available on request.

Acknowledgments

This research was supported by the National Natural Science Foundation of China (51977164), and the Office of Naval Research Global (ONRG), USA under CODE 33D, Naval Energy Resiliency and Sustainability in Broad Agency Announcement N00014-18-SB001, and ONRG award number: N62909-19-1-2037.

References

[1] Zou Y, Xu Y, Feng X, Naayagi RT, Soong B. Transactive energy systems in active distribution networks: a comprehensive review. CSEE J Electr Power Energy Syst. 2022;8(5):1302–17. https://doi.org/10.17775/CSEEJPES.2021.03290.
[2] Huang K, Yan Y, Wang G, Li B. Improving transient performance of thermoelectric generator by integrating phase change material. Energy 2021;219. https://doi.org/10.1016/j.energy.2020.119648.
[3] Hyland M, Hunter H, Liu J, Veety E, Vashaee D. Wearable thermoelectric generators for human body heat harvesting. Appl Energy 2016;182. https://doi.org/10.1016/j.apenergy.2016.08.150.
[4] Suarez F, Parekh DP, Ladd C, Vashaee D, Dickey MD, Öztürk MC. Flexible thermoelectric generator using bulk legs and liquid metal interconnects for wearable electronics. Appl Energy 2017;202. https://doi.org/10.1016/j.apenergy.2017.05.181.
[5] Zarifi S, Mirhosseini Moghaddam M. Utilizing finned tube economizer for extending the thermal power rate of TEG CHP system. Energy 2020;202. https://doi.org/10.1016/j.energy.2020.117796.
[6] Zhang Y, Wang X, Cleary M, Schoensee L, Kempf N, Richardson J. High-performance nanostructured thermoelectric generators for micro combined heat and power systems. Appl Therm Eng 2016;96. https://doi.org/10.1016/j.applthermaleng.2015.11.064.
[7] Cai Y, Wang WW, Wang L, Liu D, Zhao FY. A proton exchange membrane fuel cell-compound thermoelectric system: bidirectional modeling and energy conversion potentials. Energy Convers Manag 2020;207. https://doi.org/10.1016/j.enconman.2020.112517.
[8] Khanmohammadi S, Rahmani M, Musharavati F, Khanmohammadi S, Bach QV. Thermal modeling and triple objective optimization of a new compressed air energy storage system integrated with Rankine cycle, PEM fuel cell, and thermoelectric unit. Sustain Energy Technol Assessments 2021;43. https://doi.org/10.1016/j.seta.2020.100810.
[9] Saufi Sulaiman M, Singh B, Mohamed WANW. Experimental and theoretical study of thermoelectric generator waste heat recovery model for an ultra-low temperature PEM fuel cell powered vehicle. Energy 2019;179. https://doi.org/10.1016/j.energy.2019.05.022.
[10] Hsiao YY, Chang WC, Chen SL. A mathematic model of thermoelectric module with applications on waste heat recovery from automobile engine. Energy 2010;35. https://doi.org/10.1016/j.energy.2009.11.030.
[11] Lu H, Wu T, Bai S, Xu K, Huang Y, Gao W, et al. Experiment on thermal uniformity and pressure drop of exhaust heat exchanger for automotive thermoelectric generator. Energy 2013;54. https://doi.org/10.1016/j.energy.2013.02.067.
[12] Wang Y, Dai C, Wang S. Theoretical analysis of a thermoelectric generator using exhaust gas of vehicles as heat source. Appl Energy 2013;112. https://doi.org/10.1016/j.apenergy.2013.01.018.
[13] Rodriguez R, Guo J, Preindl M, Cotton JS, Emadi A. High frequency injection maximum power point tracking for thermoelectric generators. Energy Convers Manag 2019;198. https://doi.org/10.1016/j.enconman.2019.111832.
[14] Mamur H, Ahiska R. Application of a DC-DC boost converter with maximum power point tracking for low power thermoelectric generators. Energy Convers Manag 2015;97. https://doi.org/10.1016/j.enconman.2015.03.068.
[15] Kanagaraj N. Photovoltaic and thermoelectric generator combined hybrid energy system with an enhanced maximum power point tracking technique for higher energy conversion efficiency. Sustain 2021;13. https://doi.org/10.3390/su13063144.
[16] Montecucco A, Knox AR. Maximum power point tracking converter based on the open-circuit voltage method for thermoelectric generators. IEEE Trans Power Electron 2015;30:828–39. https://doi.org/10.1109/TPEL.2014.2313294.
[17] Vega J, Lezama J. Design and implementation of a thermoelectric energy harvester with MPPT algorithms and supercapacitor. IEEE Lat Am Trans 2021;19. https://doi.org/10.1109/TLA.2021.9423860.
[18] Park J do, Lee H, Bond M. Uninterrupted thermoelectric energy harvesting using temperature-sensor- based maximum power point tracking system. Energy Convers Manag 2014;86:233–40. https://doi.org/10.1016/j.enconman.2014.05.027.
[19] Bijukumar B, Kaushik Raam AG, Ganesan SI, Nagamani C. A linear extrapolation-based MPPT algorithm for thermoelectric generators under dynamically varying temperature conditions. IEEE Trans Energy Convers 2018;33:1641–9. https://doi.org/10.1109/TEC.2018.2830796.
[20] Bond M, Park J do. Current-sensorless power estimation and MPPT implementation for thermoelectric generators. IEEE Trans Ind Electron 2015;62:5539–48. https://doi.org/10.1109/TIE.2015.2414393.
[21] Zhang X, Tan T, Yang B, Wang J, Li S, He T, et al. Greedy search based data-driven algorithm of centralized thermoelectric generation system under non-uniform temperature distribution. Appl Energy 2020;260. https://doi.org/10.1016/j.apenergy.2019.114232.
[22] Yang B, Wang J, Zhang X, Zhang M, Shu H, Li S, et al. MPPT design of centralized thermoelectric generation system using adaptive compass search under non-uniform temperature distribution condition. Energy Convers Manag 2019;199. https://doi.org/10.1016/j.enconman.2019.111991.
[23] Li H, Yang D, Su W, Lu J, Yu X. An overall distribution particle swarm optimization MPPT algorithm for photovoltaic system under partial shading. IEEE Trans Ind Electron 2019;66:265–75. https://doi.org/10.1109/TIE.2018.2829668.
[24] Ebrahim EA. Bacteria-foraging based-control of high-performance railway level-crossing safety drives fed from photovoltaic array. J Electr Syst Inf Technol 2016;3. https://doi.org/10.1016/j.jesit.2015.11.014.
[25] Mohanty S, Subudhi B, Ray PK. A new MPPT design using grey Wolf optimization technique for photovoltaic system under partial shading conditions. IEEE Trans Sustain Energy 2016;7. https://doi.org/10.1109/TSTE.2015.2482120.
[26] Shams I, Mekhilef S, Tey KS. Maximum power point tracking using modified butterfly optimization algorithm for partial shading, uniform shading, and fast varying load conditions. IEEE Trans Power Electron 2021;36:5569–81. https://doi.org/10.1109/TPEL.2020.3029607.
[27] Cai Y, Deng F, Zhao J, Ding N, Chen J. An MPTD-specialized MPPT algorithm used for a novel medium-power thermoelectric system. IEEE Trans Power Electron 2021;36:4187–97. https://doi.org/10.1109/TPEL.2020.3023852.
[28] Montecucco A, Siviter J, Knox AR. The effect of temperature mismatch on thermoelectric generators electrically connected in series and parallel. Appl Energy 2014;123:47–54. https://doi.org/10.1016/j.apenergy.2014.02.030.
[29] Liu YH, Chiu YH, Huang JW, Wang SC. A novel maximum power point tracker for thermoelectric generation system. Renew Energy 2016;97:306–18. https://doi.org/10.1016/j.renene.2016.05.001.
[30] Fares D, Fathi M, Shams I, Mekhilef S. A novel global MPPT technique based on squirrel search algorithm for PV module under partial shading conditions. Energy Convers Manag 2021:230. https://doi.org/10.1016/j.enconman.2020.113773.
[31] Park M, Yu IK. A novel real-time simulation technique of photovoltaic generation systems using RTDS. IEEE Trans Energy Convers 2004;19. https://doi.org/10.1109/TEC.2003.821837.